Interaction of the Major Epitope Region of HIV Protein gp41 with Membrane Model Systems. A Fluorescence Spectroscopy Study†

Nuno C. Santos,‡,§ Manuel Prieto,‡ and Miguel A. R. B. Castanho*,‡,§

Centro de Química-Física Molecular, Complexo I, Instituto Superior Técnico, 1096 Lisboa Codex, Portugal, and Departamento de Química e Bioquímica, Faculdade de Ciências da Universidade de Lisboa, Campo Grande, 1700 Lisboa, Portugal

Received February 19, 1998; Revised Manuscript Received April 9, 1998

ABSTRACT: Fluorescence spectroscopy (both steady-state and time-resolved) was used to study the fragment 579−601 of gp41 ectodomain (HIV-1), a highly conserved sequence and major epitope, regarding (1) structural information, (2) interaction with membrane model systems, and (3) location in the phospholipid bilayer. The peptide was characterized both in its monomeric (after reduction of the disulfide bond between cysteine residues) and in the dimeric forms. The change of the fluorescence anisotropy between monomer and dimer was rationalized on the basis of energy migration, and a distance between the two tryptophan (Trp) residues of ≈6 Å was obtained. Using different fluorescence spectroscopy approaches, it was demonstrated that, despite the fact that monomeric gp41 fragment incorporates in the membrane model systems studied, the dimeric form does not interact with these vesicles. A methodology based on the increase of the mean fluorescence lifetime averaged by the preexponentials was derived, to obtain the partition coefficient of the peptide in the different lipid systems. Fluorescence quenching using lipophilic probes and red edge excitation shift (REES) were used to study the location of the gp41 fragment in the membrane. It was concluded that the Trp residue is located in a shallow position, near the interface. The REES results show an uncommonly large wavelength shift (18 nm) for the gp41 fragment incorporated in the membrane. Our results are consistent with a "two steps" model for the gp41 fusion mechanism similar to the one proposed for influenza virus hemagglutinin.

The envelope glycoproteins of HIV-1[1] are synthesized in the rough endoplasmic reticulum as a single precursor with an apparent molecular mass of 160 kDa (gp160), where it is also glycosylated. Afterward it is transferred to the Golgi where it is cleaved by a cellular protease into two subunits before the incorporation into a virus particle (for review, see, e.g., *1*). The surface subunit, gp120, is responsible for the recognition and attachment to the T-cell receptor (CD4) on the target cell, and to a recently discovered chemokine second receptor (*2*, *3*). The transmembrane subunit, gp41, is noncovalently bonded to gp120. It has two hydrophobic domains, one responsible for the anchoring of the gp120/gp41 complex to the viral membrane, and the other responsible for the fusion with the target cell after the recognition of CD4 by gp120. For the fusion and mixing of the cellular and viral contents to occur, gp41 must undergo a complex conformational change, apparently triggered by the gp120−CD4 attachment (*4*).

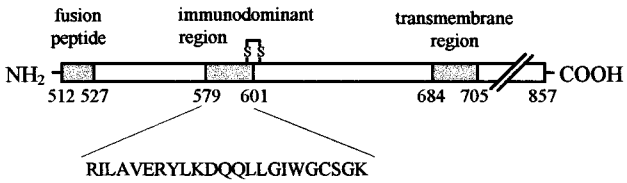

FIGURE 1: Diagram of gp41 sequence (HXB2R strain), indicating the sequence of the immunodominant region, identical to the synthetic peptide studied in this work.

Most of the therapeutical strategies against HIV are focused on the inhibition of the enzymes reverse transcriptase and HIV protease (*5*). However, the inhibition of membrane fusion by therapeutical actions on the gp120/gp41 complex is now achieving an increased importance as an alternative or additional approach to the problem. The highly conserved sequence of gp41 makes it a largely relevant target (*6*).

In the present work, we have studied a synthetic peptide (Figure 1) with 23 amino acid residues, analogous to residues 579−601 of the gp41 ectodomain (HXB2R strain), which has received recent attention in the literature. This highly conserved sequence was proven to be a major immunodominant region, recognized by antibodies from approximately 98% of AIDS patients (*7*). It was also shown by different authors that several epitopes of this region are essential for gp41 activity (*8*−*12*).

This peptide also includes the terminal sequence of an extended amphipathic α-helix, similarly to the transmembrane proteins of other retroviruses, containing a leucine zipper-like region. It was proved that peptides of this region

† This work was supported by Project PCNA/C/BIO/56/96 (Program PRAXIS XXI, MCT, Portugal) and Fundação Calouste Gulbenkian (Portugal). N.C.S. also acknowledges Grant BD 5935/95 from PRAXIS XXI.

* Address correspondence to this author at Instituto Superior Técnico.
‡ Instituto Superior Técnico.
§ Faculdade de Ciências da Universidade de Lisboa.

[1] Abbreviations: HIV-1, human immunodeficiency virus type 1; gp, glycoprotein; HA, influenza virus hemagglutinin; 5NS, 5-doxylstearic acid; 16NS, 16-doxylstearic acid; POPC, 1-palmitoyl-2-oleoylphosphatidylcholine; DMPG, dimyristoylphosphatidylglycerol; TCP, tris-(2-cyanoethyl)phosphine; PBS, phosphate-buffered saline; LUV, large unilamellar vesicles; SUV, small unilamellar vesicles; REES, red edge excitation shift.

S0006-2960(98)00393-6 CCC: $15.00
Published on Web 05/27/1998

have a strong antiviral activity, by blocking synctia formation by infected cells and infection by the free virus (*4*). It is generally accepted that the leucine zipper-like motif is responsible for the oligomerization of the transmembrane proteins, forming a coiled-coil structure (e.g., *13*). Wild et al. (*14*) suggested that, after gp120 linkage to CD4, this gp41 domain undergoes a conformational transition from a precursor structure to a coiled-coil, leading the gp120/gp41 complex to its fusogenic state and approaching the fusion domain of gp41 to the target cell.

It is the purpose of the present work to study this gp41 fragment in its dimeric and monomeric forms in aqueous solution, and their interaction with different membrane model systems. The monomer/oligomer transitions and the interaction of this gp41 domain with the target cell membrane may be of key importance in the viral fusion mechanism, as suggested for the fusion mechanism of influenza virus hemagglutinin (HA) (*15*), a protein that presents several analogies with the gp120/gp41 complex. Steady-state and time-resolved fluorescence spectroscopy were used to obtain structural information on the gp41 fragment and to evaluate its incorporation in the membrane model systems and its location in the phospholipid bilayer.

MATERIALS AND METHODS

Materials. HIV envelope protein gp41 fragment 579−601 (Arg-Ile-Leu-Ala-Val-Glu-Arg-Tyr-Leu-Lys-Asp-Gln-Gln-Leu-Leu-Gly-Ile-Trp-Gly-Cys-Ser-Gly-Lys), 5-doxylstearic acid (5NS), 16-doxylstearic acid (16NS), and 2-mercaptoethanol were obtained from Sigma (St. Louis, MO). 1-Palmitoyl-2-oleoylphosphatidylcholine (POPC) and dimyristoylphosphatidylglycerol (DMPG) were obtained from Avanti Polar Lipids (Birmingham, AL). Tris(2-cyanoethyl)phosphine (TCP) was from Molecular Probes (Eugene, OR). All the buffer salts (NaCl, KCl, KH_2PO_4, and Na_2HPO_4), L-tryptophan (Trp), and L-tyrosine (Tyr) were purchased from Merck (Darmstadt, Germany).

Sample Preparation. Dulbecco's phosphate buffered saline (PBS) solution, pH 7.4, was used throughout the studies. POPC/DMPG mixture, 80:20 (mol %), and pure DMPG vesicles were used on the studies of the interaction with membrane model systems. It was shown by differential scanning calorimetry and fluorescence spectroscopy that there is no phase separation in membranes of the POPC/DMPG mixture in the proportion used in the present work (*16*). Large unilamellar vesicles (LUV) and small unilamellar vesicles (SUV) were prepared as described elsewhere (*17*). Power sonication was carried out using a Branson Sonifier 250 (40 W) equipped with a microtip.

Direct dissolution of the peptide in a small volume of buffer was achieved by vortexing and bath sonication (Bandelin Sonorex RK 156). The solution was allowed to rest for at least 1 h before use. Peptide concentration was calculated from the absorbance at 280 and 288 nm, as described in (*18*). No presence of the Trp oxidation product kynurenine was found by UV−Vis absorption spectroscopy, with or without bath sonication. Absorbance measurements were carried out in a Jasco V-560 spectrophotometer. Peptide concentrations used in the fluorescence studies ranged from 10 to 40 mM. Reduction of the disulfide bonds between cysteine (Cys) residues was carried out by adding 2-mercaptoethanol (0.1 M, 2 h incubation) or TCP (1 mM, 1 h incubation). TCP is a recently commercialized selective disulfide reducing agent, similar to tris(2-carboxyethyl)-phosphine studied in (*19*). The use of TCP has several advantages over mercaptoethanol; namely, lower concentration and incubation time are required, it does not absorb light in the wavelength range of interest (Trp excitation), it is not an efficient quencher of Trp or Tyr fluorescence at the concentration used (results not shown), it is not pH sensitive, and it is considered more efficient in the reduction of buried disulfide bonds.

All the preparative processes involving the peptide, Trp, or Tyr solutions were carried out in the dark.

Membrane incorporation studies were performed by adding small volumes of concentrated vesicle stock solutions to the peptide samples, followed by an incubation of 30 min before measurements. Quenching studies were performed by successive additions of small amounts of 5NS or 16NS in ethanol to samples of the peptide incubated with LUV. The final ethanol concentration was kept below 2% (v/v), to avoid significant bilayer alterations (*20*). An incubation time of 15 min was kept between each increase of quencher concentration and measurement.

All fluorescence studies were carried out at room temperature using 5 mm × 5 mm quartz cuvettes.

Steady-State Fluorescence Studies. Steady-state fluorescence measurements were carried out using a SPEX F112 A Fluorolog spectrofluorometer (150 W Xe lamp and double emission monochromator). Correction of excitation and emission spectra was performed using a Rhodamine B quantum counter solution and a standard lamp, respectively (e.g., *21*). Typical spectral bandwidths were 4.5 nm for excitation and 2.25 nm for emission. All the data were corrected for background intensities, progressive dilution, and, whenever it was necessary, the inner filter effect as previously described (*22*). Emission spectra were not corrected for the photomultiplier wavelength dependence.

Fluorescence anisotropies were determined according to the equation:

$$r = \frac{I_{VV} - GI_{VH}}{I_{VV} + 2GI_{VH}} \quad (1)$$

(e.g., *21*), where I_{VV} and I_{VH} are the fluorescence intensities and the subscripts indicate the vertical (V) or horizontal (H) orientations of the excitation and emission Glan−Thompson polarizers. $G = I_{HV}/I_{HH}$ is the instrumental factor.

Fluorescence quantum yields, ϕ, were determined using Trp in water as the standard ($\phi_{Trp} = 0.16$, *23*). Bimolecular quenching rate constants, k_q, were determined either from steady-state or from time-resolved fluorescence intensities (static quenching is negligible) according to a Stern−Volmer relationship (e.g., *21*):

$$\frac{\tau_o}{\tau} = \frac{\phi_o}{\phi} = 1 + k_q\tau_o[Q] \quad (2)$$

where τ_o and ϕ_o are the fluorescence lifetime and quantum yield in the absence of quencher, respectively, and [Q] is the quencher concentration.

Time-Resolved Fluorescence Studies. Time-resolved fluorescence instrumentation was previously described (*24*).

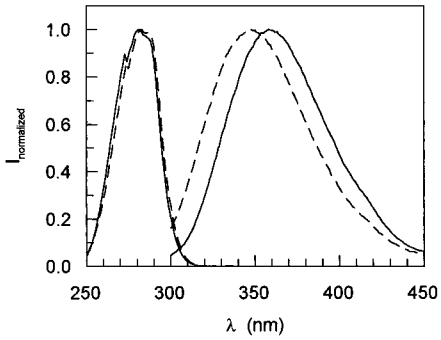

FIGURE 2: Excitation (λ_{em} = 360 nm) and emission (λ_{exc} = 280 nm) spectra of gp41 fragment 579−601 in aqueous solution (—). There is no significant change after incubation with the reducing agent (mercaptoethanol or TCP), or in the presence of phospholipid vesicles without the reducing agent. Excitation and emission spectra (same wavelengths) of the peptide, after reduction of the disulfide bonds, in the presence of DMPG SUV (− −).

Fluorescence decay measurements were carried out using a time-correlated single-photon counting system. For excitation at 300 nm, a frequency-doubled cavity-dumped dye laser of Rhodamine 6G (Coherent 701-2), synchronously pumped by a mode-locked Ar^+ laser (514.5 nm, Coherent Innova 400-10), was used. A cutoff filter (WG-360, Corion) was added to a Jobin-Yvon HR320 monochromator, to further screen scattered excitation light. For the detection, a Hamamatsu R-2809 MCP photomultiplier was used, and the instrumental response functions (80 ps fwhm) for deconvolution were generated from a scatter dispersion (Silica, colloidal water suspension; Aldrich, Milwaukee, WI). Emission (at 365 nm) was detected at the magic angle (54.7°) relative to the vertically polarized excitation beam. The number of counts on the peak channel was 20 000, and the number of channels per curve used for analysis was 300, with 11.02 or 11.04 ps/channel.

Data analysis was carried out using a nonlinear, least-squares iterative convolution method based on the Marquardt algorithm (*25*). Three exponentials were required to the fit, and its goodness was judged from the global chi-square value (χ_G^2), weighted residuals, and autocorrelation plots (e.g., *26*). For the case of a complex lifetime, described by a sum of exponentials, the average fluorescence lifetime of a fluorophore, $\langle\tau\rangle$, is

$$\langle\tau\rangle = \frac{\sum a_i \tau_i^2}{\sum a_i \tau_i} \qquad (3)$$

(e.g., *21*), where τ_i represents each component of the fluorescence lifetime and a_i the respective pre-exponential factor, which is proportional to the concentration of the component.

RESULTS

Photophysical Characterization in Aqueous Solution. Due to the presence of a single Cys residue, it is expected that gp41 fragment 579−601 in solution adopts the dimeric form by intermolecular disulfide bonding. The spectral characteristics of the peptide are dominated by the single Trp residue. The normalized excitation and emission fluorescence spectra of the peptide are presented in Figure 2. In solution, it has an absorbance maximum at 280 nm, and an emission maximum at 360 nm when excited at the absorbance maximum. These values are coincident with those obtained for free Trp in buffer under the same experimental conditions. Upon reduction of the disulfide bond (either by mercaptoethanol or by TCP; monomerization) or power sonication of the peptide solution, no spectral alteration could be noticed.

Table 1: Fluorescence Lifetime Parameters Obtained for gp41 Fragment 579−601 in the Presence and Absence of Mercaptoethanol (merc) (Reducing Agent) and Lipid (L)[a]

[merc] (M)	[L] (mM)	$\langle\tau\rangle$ (ns)	a_1	τ_1 (ns)	a_2	τ_2 (ns)	a_3	τ_3 (ns)
0	0	3.50	0.16	0.35	0.29	1.68	0.55	3.99
0.1	0	2.47	0.18	0.33	0.38	1.55	0.44	2.97
0.1	5.8[b]	3.23	0.23	0.34	0.45	1.85	0.32	4.25
0.1	5.8[c]	3.28	0.25	0.49	0.51	2.01	0.24	4.74

[a] The values of $\langle\tau\rangle$ were calculated using eq 3. [b] POPC/DMPG 80:20. [c] DMPG

The fluorescence decay of the dimeric peptide upon excitation of the Trp chromophore (λ_{exc} = 300 nm) is described by a sum of not less than three exponentials (Table 1), with a mean lifetime $\langle\tau\rangle$ = 3.50 ns. In the presence of mercaptoethanol (0.1 M), this value is reduced to $\langle\tau\rangle$ = 2.47 ns. To discriminate if this effect is either due to an alteration of the peptide structure upon monomerization or results from the reducing agent acting as a quencher, a steady-state fluorescence study of the quenching of Trp (as a model compound of Trp in the peptide) by mercaptoethanol was carried out. From eq 2, a value of $k_q = 1.6 \times 10^9$ M^{-1} s^{-1} was recovered. This is close to the value obtained for the peptide using transient state data, $k_q = 1.2 \times 10^9$ M^{-1} s^{-1}, when mean lifetimes of the peptide in the absence (dimer) and presence of mercaptoethanol (monomer) are considered.

The values of fluorescence anisotropy for the monomeric and dimeric species are r_{mon} = 0.027 and r_{dim} = 0.024. The dimer quantum yield (λ_{exc} = 290 nm) is ϕ_{dim} = 0.13.

Photophysical Characterization in Membrane Model Systems. The interaction of the peptide both with SUV and with LUV could be followed by the changes in several spectroscopic parameters, namely, fluorescence intensity, spectral shifts, and fluorescence lifetime, but none of these could detect any interaction between gp41 fragment in the dimeric form (i.e., previous to reduction of the disulfide bond) and vesicles of POPC/DMPG mixture 80:20 or pure DMPG. At variance, the incorporation of the monomeric peptide (i.e., after reduction of the disulfide bond) with membrane model systems could be detected by the three different fluorescence spectroscopy approaches. As shown in Figure 2, there is a significant blue-shift of the emission spectra of the monomeric fragment of gp41 in the presence of phospholipid vesicles. The effect is larger for pure DMPG vesicles, and there are no significant changes in the excitation spectra. This spectral shift is known to be due to the incorporation in a more hydrophobic environment. This is confirmed by fluorescence intensities and lifetimes, as will be shown below. A concomitant increase of the mean lifetime of the monomeric species is observed in the presence of lipid (Table 1), when compared with the value obtained in aqueous solution. There was no significant difference between the results obtained with SUV and LUV. Evidence of membrane incorporation was also obtained after power sonication of

the peptide in the dimeric form in the presence of phospholipid vesicles.

Determination of the Partition Coefficient. The partition coefficient between the lipid and aqueous phases, K_p, described by the equation

$$K_p = \frac{n_L/V_L}{n_W/V_W} \quad (4)$$

was determined in order to quantify the extent of interaction of the peptide with the membrane model system (e.g., *27*). In this equation, n is the moles of peptide, V is the volume of the phase, and the subscripts L and W refer to the lipid and water phases, respectively. In this work, the partition coefficients of the gp41 fragment were obtained by two methods, both based on the changes of its spectroscopic parameters between the lipid and aqueous phases. The partition coefficients of the peptide in the lipidic systems can be obtained from fluorescence intensity data, I, using eq 5, derived in (*28*).

$$I - I_w = \frac{(I_L - I_W)K_p\gamma_L[L]}{1 + K_p\gamma_L[L]} \quad (5)$$

I_W and I_L are the limit fluorescence intensities with all the peptide in water and in the lipid phase, respectively, γ_L is the molar volume of the phospholipid, and [L] is the lipid concentration. Plotting the values of $I - I_W$ obtained after incubation with different lipid concentrations versus [L], and performing a nonlinear regression, K_p and I_L are obtained. Fluorescence intensity data obtained using SUV of POPC/DMPG 80:20 are presented in Figure 3a. Values of $K_p = (1.4 \pm 0.8) \times 10^2$ and $I_L/I_W = 1.9 \pm 1.4$ were obtained, considering $\gamma_{POPC} = 0.762\ M^{-1}$ and $\gamma_{DMPG} = 0.519\ M^{-1}$ (*29*).

As depicted in Figure 3a, the experimental data quality obtained using this methodology (steady-state fluorescence intensities) is poor. This is eventually due to the difficulty of measuring precise intensities in the presence of significant light scattering caused by the vesicle suspension. This prompted us to derive a methodology based on fluorescence lifetime measurements, where this artifact is avoided. The methodology is based on the increase of the mean fluorescence lifetime upon increasing lipid concentration. Using the average fluorescence lifetime, $\langle\tau\rangle$, calculated using eq 3, the following relationship is obtained (derivation not shown):

$$\langle\tau\rangle = \langle\tau\rangle_W + (\langle\tau\rangle_L - \langle\tau\rangle_W)\frac{K_p\gamma_L[L]}{K_p\gamma_L[L] + \epsilon_W\phi_W/(\epsilon_L\phi_L)} \quad (6)$$

This methodology requires independent knowledge of the ratio obtained by steady-state fluorescence spectroscopy:

$$\frac{\epsilon_W\phi_W}{\epsilon_L\phi_L} = \frac{I_W}{I_L} \quad (7)$$

where ϵ is the molar absorptivity. To avoid the error associated with its determination, we have derived another formalism based instead on the fluorescence lifetime averaged by the preexponentials:

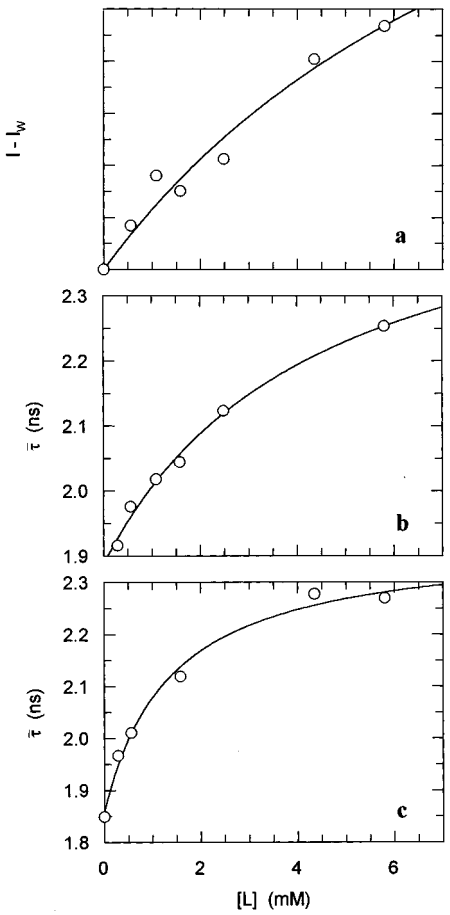

FIGURE 3: Determination of the partition constant (K_p) of the peptide between the aqueous phase and phospholipid vesicles. Peptide concentration was constant during each set of experiments. Increase in fluorescence intensity ($I - I_W$) obtained for different concentrations of POPC/DMPG 80:20 SUV (a), and fitting lines calculated using eq 5. Fluorescence lifetime averaged by the pre-exponentials ($\bar{\tau}$) obtained for different concentrations of POPC/DMPG 80:20 (b) and pure DMPG (c) SUV, and fitting lines calculated using eq 9.

$$\bar{\tau} = \frac{\sum a_i\tau_i}{\sum a_i} \quad (8)$$

This is an additive parameter and, therefore, the formalism is simpler. As derived in Appendix I, the following relationship is obtained:

$$\bar{\tau} = \frac{\bar{\tau}_W + \bar{\tau}_L K_p\gamma_L[L]}{1 + K_p\gamma_L[L]} \quad (9)$$

where $\bar{\tau}_W$ and $\bar{\tau}_L$ are the fluorescence lifetimes averaged by the pre-exponentials regarding the peptide in the aqueous phase and in the membrane, respectively. By nonlinear fit of $\bar{\tau}$ versus [L] data, we obtain K_p and $\bar{\tau}_L$. Data obtained for the incorporation of the gp41 fragment in POPC/DMPG 80:20 vesicles using this methodology are presented in Figure 3b. The recovered $K_p = (3.1 \pm 1.0) \times 10^2$ is slightly higher than the one previously obtained, although the error ranges overlap. To compare the incorporation in both lipid systems, this methodology was also applied to pure DMPG vesicles (Figure 3c). The values of K_p, $\bar{\tau}_W$, and $\bar{\tau}_L$ obtained for both systems are presented in Table 2.

Table 2: Parameters Obtained Using Eq 9 for the gp41 Fragment Interaction with SUV of 80:20 POPC/DMPG Mixture and Pure DMPG

lipid	$K_p/10^2$	$\bar{\tau}_L$ (ns)	$\bar{\tau}_W$ (ns)
POPC/DMPG	3.1 ± 1.0	2.54 ± 0.09	1.88 ± 0.02
DMPG	14.1 ± 3.8	2.38 ± 0.04	1.86 ± 0.02

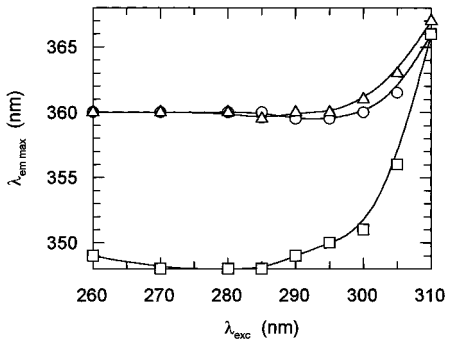

FIGURE 4: Red-edge excitation shift (REES). Wavelengths of the maxima of the emission spectra obtained at different excitation wavelengths for the peptide in the dimeric (○) and monomeric (△) forms in aqueous solution, and for the peptide in the monomeric form in DMPG SUV 5.8 mM (□). The lines connecting experimental data are merely guides to the eye.

Red Edge Excitation Shift. The red edge excitation shift (REES) can be described as the increase in the wavelength of maximum emission observed when the excitation wavelength is gradually shifted towards the red edge of the absorption band (for review, see *30*). A concomitant increase of fluorescence anisotropy is also observed. This phenomenon is usually observed for motionally restricted polar fluorophores. Thus, REES can be used to obtain information on the nature of the environment of the fluorophore, including Trp residues in proteins (e.g., *31*, *32*) and in peptides interacting with membranes (*33*−*35*). The variations of the wavelength of maximum emission with the increase of the excitation wavelength for the gp41 fragment in the dimeric form, after reduction (monomeric) and in the presence of DMPG SUV, are presented in Figure 4. A larger REES is clearly observed for the peptide incorporated in the bilayer.

Fluorescence Quenching by Lipophilic Probes. To evaluate the localization of the Trp residue of the gp41 fragment when it is interacting with the membrane model system, fluorescence quenching by the lipophilic probes 5NS and 16NS was used. These two derivatized fatty acids differ in the position of the quencher moiety (doxyl) in the hydrocarbon chain. Thus, they are used to evaluate the depth of the fluorophore in the membrane, by comparing the quenching results obtained with each of them (e.g., *36*, *37*). The steady-state fluorescence quenching measurements were performed with fixed concentrations of peptide and lipid, and increasing concentration of quencher. The effective quencher concentration in the membrane, $[Q]_L$, was calculated using the following relationship (*38*):

$$[Q]_L = [Q]_T\left(1 - \frac{K_{p,Q}\gamma_L[L]}{1 - \gamma_L[L] + K_{p,Q}\gamma_L[L]}\right)\frac{K_{p,Q}}{1 - \gamma_L[L]} \quad (10)$$

where $[Q]_T$ is the total quencher concentration and $K_{p,Q}$ is the partition coefficient of the quencher. The $K_{p,Q}$ values used were 12 570 and 3340 for 5NS and 16NS, respectively, as reported in (*39*) for dipalmitoylphosphatidylcholine unilamellar vesicles. Considering that there is a fluorophore population A protected from contact with the quencher, and a population B accessible to it, the fluorescence quenching data were analyzed using a direct fit (*22*) of the Lehrer equation (*40*):

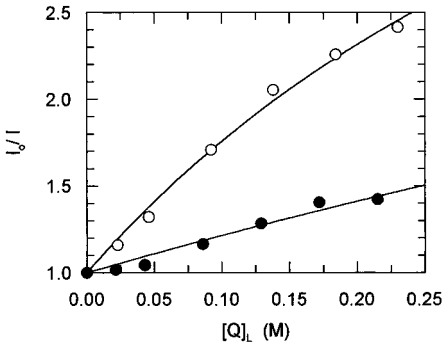

FIGURE 5: Fluorescence quenching of the peptide in DMPG SUV 5.8 mM. Variation of I_o/I with the increase of the effective concentration of 5NS (○) and 16NS (●), and fitting lines obtained using eq 11.

$$\frac{I_o}{I} = \frac{1 + K_{SV}[Q]_L}{(1 + K_{SV}[Q]_L)(1 - f_B) + f_B} \quad (11)$$

In this equation, I_o is the fluorescence intensity in the absence of quencher, K_{SV} is the Stern−Volmer quenching constant (e.g., *21*), and

$$f_B = \frac{I_{o,B}}{I_o} \quad (12)$$

where $I_{o,B}$ is the fluorescence intensity of the fluorophore population accessible to the quencher. The variation of I_o/I with the increase of the effective concentration of 5NS and 16NS is presented in Figure 5, together with the fitting lines obtained using eq 11. For the quenching with 5NS, the values of $K_{SV} = 10.8 \pm 1.4\ M^{-1}$ and $f_B = 0.83 \pm 0.04$ were obtained. This last value is in close agreement with the fraction of the fluorescence intensity emitted by the peptide incorporated in the membrane at the lipid concentration used ($f_L = 0.87$). Therefore, all the peptide in the membrane is accessible to the quencher. The value of f_L was calculated using eq 13 (derived in Appendix II), and the values of K_p and I_L/I_W previously obtained.

$$f_L = \frac{(I_L/I_W)K_p\gamma_L[L]}{1 + (I_L/I_W)K_p\gamma_L[L]} \quad (13)$$

For the quenching with 16NS, a lower value of $K_{SV} = 2.7 \pm 0.1\ M^{-1}$ was obtained for the same f_B value. The shift in the emission spectra to higher wavelengths in the presence of the quencher, as shown in Figure 6, further confirms the preferential quenching of the Trp residues in the bilayer and the greater ability of 5NS to quench the fluorophores.

DISCUSSION

gp41 Fragment 579−*601 in Aqueous Solution.* Both the fluorescence emission (Figure 2) spectrum and the mean fluorescence lifetime of the peptide $\langle\tau\rangle = 3.50$ ns (Table 1)

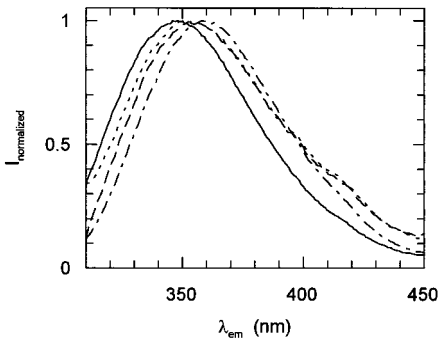

FIGURE 6: Emission spectra (λ_{exc} = 280 nm) of gp41 fragment 579−601 in DMPG SUV with 5NS (- - -) and 16NS (− −). For the sake of comparison, the spectra of the peptide in DMPG SUV without quencher (—) and in water (− - −) are also shown. The shifts in the spectra to higher wavelengths confirm the preferential quenching of the Trp residues in the bilayer by the NS, and the larger ability of 5NS to quench these fluorophores.

are similar to those of Trp in aqueous solution. The single Trp lifetime is expectedly complex (described by a sum of three exponentials), this being ascribed to the existence of distinct conformers (e.g., *41*, *42*). Its apparent decrease to $\langle\tau\rangle = 2.47$ ns upon monomerization is due to the quenching ability of the reducing agent (mercaptoethanol), and not due to any structural alteration. In fact, upon comparison of the monomer and dimer fluorescence lifetimes, the bimolecular quenching rate constant obtained ($k_q = 1.2 \times 10^9$ M^{-1} s^{-1}) is close to the one obtained for Trp in a steady-state experiment ($k_q = 1.6 \times 10^9$ M^{-1} s^{-1}). From these values, it can be concluded that the Trp fluorescence quenching by mercaptoethanol is a close to diffusion-controlled process ($k_q = 7.4 \times 10^9$ M^{-1} s^{-1}, *43*, is the Smoluchowski−Stokes−Einstein collisional rate constant in water at 25 °C for small molecules). In addition, upon comparison of the time-resolved and steady-state values, it can be inferred that no significant static quenching (i.e., fluorophore−quencher complex formation) occurs.

The dimer fluorescence anisotropy can be rationalized on the basis of energy migration between the two Trp residues. Considering the Perrin equation (e.g., *21*)

$$r = \frac{r_o}{1 + \tau/\Phi} \tag{14}$$

where r_o is the intrinsic anisotropy and Φ the rotational correlation time, defined as

$$\Phi = \frac{\eta V}{RT} \tag{15}$$

once it is assumed that the Einstein equation (approximation to a spherical molecule) is valid and the volume, V, of the dimer is the double of the monomer, the following relationship between the dimer and monomer anisotropies is derived:

$$r_{dim} = r_{mon}\frac{\Phi_{mon} + \tau_{mon}}{\Phi_{mon} + \tau_{dim}/2} \tag{16}$$

The monomer rotational correlation time is $\Phi_{mon} = 0.56$ ns, assuming $V_{mon} = 2576$ Å^3 calculated from the van der Waals increments of atoms or groups (*44*), and $\eta = 0.89$ cP (25 °C). Thus, the variation of both volume and lifetime from the monomer to the dimer is taken into account, and it is calculated that $r_{dim} = 0.036$. The value is greater than the experimental one, $r_{dim} = 0.024$, revealing the existence of energy migration between the Trp residues of the two monomers, a factor not accounted for when deriving eq 16. This photophysical interaction decreases the observed anisotropy of the system, and for a cluster of two molecules (dimer), its value is (*45*)

$$r = r_1\frac{1 + (R_o/l)^6}{1 + 2(R_o/l)^6} + r_{et}\frac{(R_o/l)^6}{1 + 2(R_o/l)^6} \tag{17}$$

where l is the distance between the two chromophores, R_o is the Förster radius of the system, r_1 is the anisotropy of the initially excited molecule ($r = 0.036$ in the present experiment), and r_{et} is the anisotropy of the second molecule of the pair. This latter value is always less than 4% of the total anisotropy; thus, the second term in eq 17 can be neglected. For this particular system, it is calculated from the last equation that $l \approx R_o$; i.e., the distance between the two Trp residues is close to the Förster radius. For Trp with a quantum yield $\phi = 0.13$, this value is about 6 Å (*46*). As the chromophores are in close contact, an eventual additional contribution of an exchange mechanism of energy transfer (*47*) cannot be discarded.

The previous reasoning is based on simplifying assumptions (mean lifetime and spherical rotor were considered), and the anisotropy values are slightly biased due to a small contribution of indirectly excited Trp via Tyr residues at λ_{exc} =280 nm due to energy transfer (e.g., *48*). However, the existence of dimers is clearly concluded. Furthermore, the short distance between the two Trp residues shows that the two dimerized peptides have a parallel conformation, indicating that this system can be a good model for the oligomeric structure to be discussed later.

Interaction with Membrane Model Systems. The different fluorescence spectroscopy methodologies clearly show that gp41 fragment 579−601 on the dimeric form (previous to reduction of the disulfide bonds) does not incorporate in the membrane model systems studied, independently of the use of SUV or LUV of POPC/DMPG 80:20 or pure DMPG. The dimeric peptide could only be incorporated by power sonication in the presence of the phospholipid vesicles. At variance, the direct incorporation of the monomer (after reduction) was demonstrated by the increase in fluorescence intensity (steady-state fluorescence) and mean lifetime (time-resolved fluorescence), and by the blue-shift of the emission spectra. The partition coefficients obtained by the methodology derived in Appendix I show a membrane incorporation of the peptide approximately 4.5 times larger when pure DMPG vesicles were used. This result was already expected, due to the positive net charge of the peptide (four positively and only two negatively charged residues). The use of pure DMPG (negatively charged phospholipid headgroup) increases the electrostatic component of the peptide partition constant and might stabilize its structure upon membrane incorporation (*49*).

Localization in the Membrane. According to the models usually accepted for the red-edge excitation shift (*30*), the large REES observed upon incorporation of the gp41 fragment in the membrane indicates that the Trp residue is localized in a region that offers an important resistance to

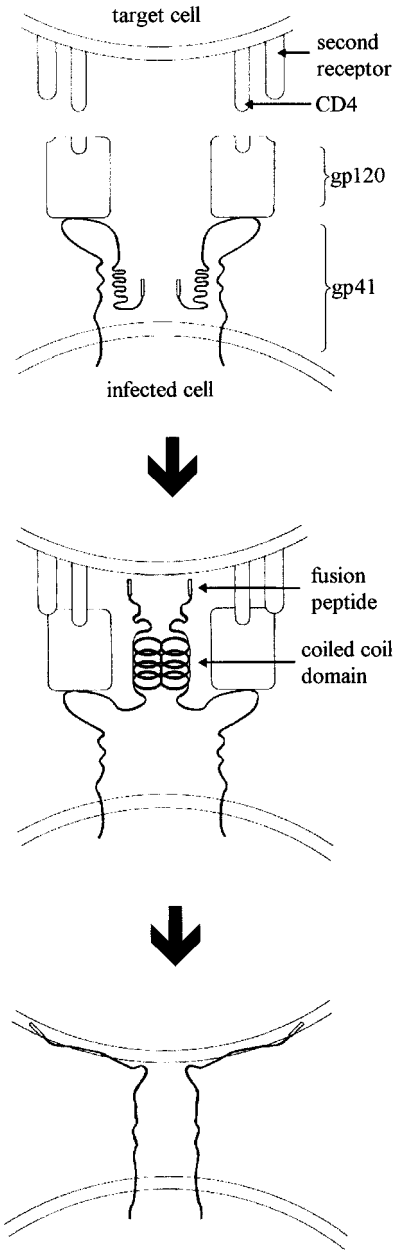

FIGURE 7: Simplified representation of the "two steps" model for the gp120/gp41 mechanism of fusion. After gp120 binding to CD4 and second receptor, gp41 undergoes several changes, including oligomerization, formation of the coiled-coil domain, and "projection" of the fusion domain toward the target cell (*14*). The insertion of the fusion peptide in the target membrane might lead to a second conformational change, with the disaggregation of the gp41 oligomer. The coiled-coil precursor region of each gp41 monomer, including the sequence studied in the present work, is inserted in the target cell bilayer interface, bringing the two membranes together and contributing to the formation of the fusion pore.

solvent reorientation. This motionally restricted environment is consistent with a location in a region near the membrane interface, involved in charge interactions and hydrogen bonding (*33*). The REES results observed in the present work are quite uncommon, not only due to the large wavelength shift (18 nm) but mainly due to the observation of REES for a peptide with the emission maximum at 348 nm when excited at the absorption maximum. This result is at variance with the generally accepted idea that REES can only be found for Trp residues emitting between 325 and 341 nm (*31*). This matter is currently under study.

Fluorescence quenching data show that the gp41 fragment is more quenched (larger K_{SV} value) by the doxyl group in 5NS than in 16NS. Thus, it can be reasoned that the fluorophore is located in a shallow position, near the interface, in agreement with REES results. The quenching data could be worked out to determine distances (*36*), or local quencher concentrations (*37*), but no significant additional information would be obtained. The only Trp residues that are not accessible to the 5NS quencher are from the fraction of the peptide remaining in aqueous solution, nonincorporated in the membranes. This location of the Trp residue is in agreement with its ability for both hydrophobic and polar interactions, and highest position on the experimental scales for the partition of amino acid residues to bilayer interfaces (*49*, *50*). However, it must be stressed that from the present work it cannot be concluded whether the peptide is transmembrane or oriented parallel to the bilayer in the interface, but only that the Trp residue is located in the interface.

Conclusions and Biochemical Relevance. The differences between monomer and oligomer (not necessarily dimer) interaction with the membrane are of key importance for the viral fusion mechanism. Considering the results obtained in this work, together with previous results by other groups, a "two steps" model can be reasoned (Figure 7), similar to the one proposed by Yu et al. (*15*) for HA fusion. As is commonly accepted, after gp120 binding to CD4, gp41 undergoes several changes, including oligomerization, formation of the coiled-coil domain, and "projection" of the fusion domain toward the target cell (*14*). A second conformational change after insertion of the fusion peptide in the target membrane can be expected, with the disaggregation of the gp41 oligomer. The coiled-coil precursor region of each gp41 monomer, including the sequence studied in the present work, is inserted in the target cell bilayer interface, bringing the two membranes together and leading to the formation of the fusion pore. This is consistent with our finding that only the monomer incorporates in the membrane and with its location. The electron paramagnetic resonance results obtained by Rabenstein and Shin (*13*) with two peptides of a region close to that studied in this work further support this kind of model. The inhibition of gp41 activity by synthetic peptides analogous to the studied region (*4*) is explained by the binding of the peptide to the corresponding sequence on gp41, making it impossible for one (or both) of the "steps" in the model to occur: the coiled-coil formation by oligomerization of the domains or its insertion in the bilayer to bring the two membranes together.

ACKNOWLEDGMENT

We thank L. M. S. Loura and Dr. A. Fedorov for technical assistance on the time-resolved fluorescence spectroscopy measurements.

APPENDIX I

Considering the total volume of the sample equal to the aqueous phase volume, $V_T \approx V_W$, and using the total moles of solute, n_T, eq 4 is written as

$$K_p = \frac{n_L/V_L}{(n_T - n_L)/V_T} \qquad \text{(AI.1)}$$

From the molar fraction, $X_i = n_i/n_T$, is obtained

$$X_L = \frac{K_p V_L}{V_T + K_p V_L} \quad \text{(AI.2)}$$

The fluorescence lifetime averaged by the pre-exponential, $\bar{\tau}$, is an additive parameter. Thus, we can separate it into the components related to each phase:

$$\bar{\tau} = \frac{\sum a_i \tau_\iota}{\sum a_i} = \frac{\sum a_{i,W}\tau_{i,W} + \sum a_{i,L}\tau_{i,L}}{\sum a_{i,W} + \sum a_{i,L}}$$

$$= \frac{\sum a_{i,W}\dfrac{\sum a_{i,W}\tau_{i,W}}{\sum a_{i,W}} + \sum a_{i,L}\dfrac{\sum a_{i,L}\tau_{i,L}}{\sum a_{i,L}}}{\sum a_{i,W} + \sum a_{i,L}} \quad \text{(AI.3)}$$

Considering

$$\sum a_{i,j} = a_j \quad \text{(AI.4)}$$

and

$$\frac{\sum a_{i,j}\tau_{i,j}}{\sum a_{i,j}} = \bar{\tau}_j \quad \text{(AI.5)}$$

eq AI.3 is converted into

$$\bar{\tau} = \frac{a_W\bar{\tau}_W + a_L\bar{\tau}_L}{a_W + a_L} \quad \text{(AI.6)}$$

As the pre-exponentials are proportional to concentration, this equation can be reformulated as

$$\bar{\tau} = X_W\bar{\tau}_W + X_L\bar{\tau}_L = \bar{\tau}_W + X_L(\bar{\tau}_L - \bar{\tau}_W) \quad \text{(AI.7)}$$

Using eq AI.2 and making $V_L = \gamma_L[L]V_T$, we obtain

$$\bar{\tau} = \frac{\bar{\tau}_W + \bar{\tau}_L K_p \gamma_L[L]}{1 + K_p\gamma_L[L]} \quad \text{(AI.8)}$$

APPENDIX II

Considering f_L, the fraction of the fluorescence intensity emitted by the fluorophore on the lipidic phase,

$$f_L = \frac{\epsilon_L\phi_L X_L}{\epsilon_L\phi_L X_L + \epsilon_W\phi_W X_W} = \frac{(\epsilon_L\phi_L/(\epsilon_W\phi_W))X_L}{(\epsilon_L\phi_L/(\epsilon_W\phi_W))X_L + X_W} \quad \text{(AII.1)}$$

As $\epsilon_L\phi_L/(\epsilon_W\phi_W) = I_L/I_W$ and $X_W = 1 - X_L$, the previous equation can be rewritten as

$$f_L = \frac{(I_L/I_W)X_L}{1 + [(I_L/I_W) - 1]X_L} \quad \text{(AII.2)}$$

Based on eq AI.2, the following relationship is easily obtained:

$$X_L = \frac{K_p\gamma_L[L]}{1 + K_p\gamma_L[L]} \quad \text{(AII.3)}$$

Using eq AII.3, eq AII.2 is reformulated as

$$f_L = \frac{(I_L/I_W)K_p\gamma_L[L]}{1 + (I_L/I_W)K_p\gamma_L[L]} \quad \text{(AII.4)}$$

REFERENCES

1. Freed, E. O., and Martin, M. A. (1995) *J. Biol. Chem. 270*, 23883−23886.
2. D'Souza, M. P., and Harden, V. A. (1996) *Nat. Med. 2*, 1293−1300.
3. Wilkinson, D. (1996) *Curr. Biol. 6*, 1051−1053.
4. Wild, C., Oas, T., McDanal, C., Bolognesi, D., and Matthews, T. (1992) *Proc. Natl. Acad. Sci. U.S.A. 89*, 10537−10541.
5. Fréchet, D., Guitton, J. D., Herman, F., Faucher, D., Helynck, G., du Sorbier, B. M., Ridoux, J. P., James-Surcouf, E., and Vuilhorgne, M. (1994) *Biochemistry 33*, 42−50.
6. Purtscher, M., Trkola, A., Gruber, G., Buchacher, A., Predl, R., Steindl, F., Tauer, C., Berger, R., Barrett, N., Jungbauer, A., and Katinger, H. (1994) *AIDS Res. Hum. Retroviruses 10*, 1651−1658.
7. Wang, J. J. G., Steel, S., Wisnielowski, R., and Wang, C. Y. (1986) *Proc. Natl. Acad. Sci. U.S.A. 83*, 6159−6163.
8. Kemp, B. E., Rylatt, D. B., Bundesen, P. G., Doherty, R. R., McPhee, D. A., Stapleton, D., Cottis, L. E., Wilson, K., John, M. A., Khan, J. M., Dinh, D. P., Miles, S., and Hillyard, C. J. (1988) *Science 241*, 1352−1354.
9. Norrby, E., Parks, D. E., Utter, G., Houghten, R. A., and Lerner, R. A. (1989) *J. Immunol. 143*, 3602−3608.
10. Sattentau, Q. J., and Moore, J. P. (1991) *J. Exp. Med. 174*, 407−415.
11. Oldstone, M. B. A., Tishon, A., Lewicki, H., Dyson, H. J., Feher, V. A., Assa-Munt, N., and Wright, P. E. (1991) *J. Virol. 65*, 1727−1734.
12. Neurath, A. R., Strick, N., and Jiang, S. (1992) *Virology 188*, 1−13.
13. Rabenstein, M. D., and Shin, Y.-K. (1996) *Biochemistry 35*, 13922−13928.
14. Wild, C., Dubay, J. W., Greenwell, T., Baird, T., Jr., Oas, T. G., McDanal, C., Hunter, E., and Matthews, T. (1994) *Proc. Natl. Acad. Sci. U.S.A. 91*, 12676−12680.
15. Yu, Y. G., King, D. S., and Shin, Y.-K. (1994) *Science 266*, 274−276.
16. Lopes, A. M. G. (1997) *Partição de xenobióticos orgânicos em agregados anfifílicos* (Ph.D. Thesis), Universidade Nova de Lisboa, Lisbon, Portugal.
17. Szoka, F., and Papahadjopoulos, D. (1980) *Annu. Rev. Biophys. Bioeng. 9*, 467−508.
18. Edelhoch, H. (1967) *Biochemistry 6*, 1948−1954.
19. Burns, J. A., Butler, J. C., Moran, J., and Whitesides, G. M. (1991) *J. Org. Chem. 56*, 2648−2650.
20. Chalpin, D. E., and Kleinfeld, A. M. (1983) *Biochim. Biophys. Acta 731*, 465−474.
21. Lakowicz, J. R. (1983) *Principles of fluorescence spectroscopy*, Plenum Press, New York.
22. Coutinho, A., and Prieto, M. (1993) *J. Chem. Educ. 70*, 425−428.
23. Kirby, E. P., and Steiner, R. F. (1970) *J. Phys. Chem. 74*, 4480−4490.
24. Loura, L. M. S., Fedorov, A., and Prieto, M. (1996) *Biophys. J. 71*, 1823−1836.
25. Marquardt, D. W. (1963) *J. Soc. Ind. Appl. Math. (SIAM J.) 11*, 431−441.
26. O'Connor, D. V., and Phillips, D. (1984) *Time-correlated single photon counting*, Academic Press, London, U.K.
27. Castanho, M. A. R. B., and Prieto, M. J. E. (1992) *Eur. J. Biochem. 207*, 125−134.
28. Coutinho, A., and Prieto, M. (1995) *Biophys. J. 69*, 2541−2557.
29. Marsh, D. (1990) *CRC handbook of lipid bilayers*, CRC Press, Boca Raton, FL.
30. Mukherjee, S., and Chattopadhyay, A. (1995) *J. Fluoresc. 5*, 237−246.
31. Demchenko, A. P. (1988) *Eur. Biophys. J. 16*, 121−129.

32. Guha, S., Rawat, S. S., Chattopadhyay, A., and Bhattacharyya, B. (1996) *Biochemistry 35*, 13426−13433.
33. Chattopadhyay, A., and Rukmini, R. (1993) *FEBS Lett. 335*, 341−344.
34. Mukherjee, S., and Chattopadhyay, A. (1994) *Biochemistry 33*, 5089−5097.
35. Ghosh, A. K., Rukmini, R., and Chattopadhyay, A. (1997) *Biochemistry 36*, 14291−14305.
36. Chattopadhyay, A., and London, E. (1987) *Biochemistry 26*, 38−45.
37. Castanho, M., Prieto, M., and Acuña, A. U. (1996) *Biochim. Biophys. Acta 1279*, 164−168.
38. Castanho, M., and Prieto, M. (1995) *Biophys. J. 69*, 155−168.
39. Wardlaw, J. R., Sawyer, W. H., and Ghiggino, K. P. (1987) *FEBS Lett. 223*, 20−24.
40. Lehrer, S. S. (1971) *Biochemistry 10*, 3254−3263.
41. Beechem, J. M., and Brand, L. (1985) *Annu. Rev. Biochem. 54*, 43−71.
42. McLaughlin, M. L., and Barkley, M. D. (1997) *Methods Enzymol. 278*, 190−202.
43. Murov, S. L., Carmichael, I., and Hug, G. L. (1993) *Handbook of photochemistry*, 2nd ed., Marcel Dekker Inc., New York.
44. Edward, J. T. (1970) *J. Chem. Educ. 47*, 261−270.
45. Runnels, L. W., and Scarlata, S. F. (1995) *Biophys. J. 69*, 1569−1583.
46. Eisinger, J., Feuer, B., and Lamola, A. A. (1969) *Biochemistry 8*, 3908−3915.
47. Dexter, D. L. (1953) *J. Chem. Phys. 21*, 836−850.
48. Moreno, M. J., and Prieto, M. (1993) *Photochem. Photobiol. 57*, 431−437.
49. Thorgeirsson, T. E., Russell, C. J., King, D. S., and Shin, Y.-K. (1996) *Biochemistry 35*, 1803−1809.
50. Wimley, W. C., and White, S. H. (1996) *Nat. Struct. Biol. 3*, 842−848.

BI9803933